Robust Block Copolymer Mask for Nanopatterning Polymer Films

Chia-Cheng Chao,[†] Tzu-Chung Wang,[‡] Rong-Ming Ho,[†,‡,*] Prokopios Georgopanos,[§] Apostolos Avgeropoulos,[§,*] and Edwin L. Thomas[⊥]

[†]Institute of Nanoengineering and Microsystems, National Tsing Hua University, Hsinchu 30013, Taiwan, R.O.C., [‡]Department of Chemical Engineering, National Tsing Hua University, Hsinchu 30013, Taiwan, R.O.C., [§]Department of Materials Science & Engineering, University of Ioannina, University Campus Ioannina 45110, Greece, and [⊥]Department of Materials Science and Engineering, Massachusetts Institute of Technology, Cambridge, Massachusetts 02139

ABSTRACT The formation of well-oriented cylinders with perpendicular morphology for polystyrene-*b*-polydimethylsiloxane (PS-PDMS) thin films was achieved by spin coating. The self-assembled PS-PDMS nanostructured thin films were used as templates for nanopatterning; the PDMS blocks can be oxidized as silicon oxy carbide microdomains, whereas the PS blocks were degenerated by a simple oxygen plasma treatment for one-step oxidization. As a result, freestanding silicon oxy carbide thin films with hexagonally packed nanochannels were directly fabricated and used as masks for pattern transfer to underlying polymeric materials by oxygen reaction ion etching (RIE) to generate topographic nanopatterns. By taking advantage of robust property and high etching selectivity of the SiOC thin films under oxygen RIE, this nanoporous thin film can be used as an etch-resistant and reusable mask for pattern transfer to various polymeric materials. This approach demonstrates a simple, convenient, and cost-effective nanofabrication technique to create the topographic nanopatterns of polymeric materials.

*Address correspondence to rmho@mx.nthu.edu.tw, aavger@cc.uoi.gr.

Nanopatterning, the fabrication of patterns with nanoscale features, has drawn great attention during the past decade. Large-sized, well-oriented periodic nanoarrays from nanopatterning are important for many practical applications.[1] To create well-defined nanopatterns over large areas, a variety of patterning technologies (including top-down and bottom-up methods) have been developed.[2] Nanopatterning based on the bottom-up method has been considered as a candidate to substitute or improve the top-down method so as to enable a variety of nanotechnologies. In particular, fabricating well-defined nanostructures for nanopatterning using the self-assembly of block copolymers (BCPs) is of great interest because of the tunable dimensions and chemical properties with a flexible, simple, and low-cost process.[3,4] Many potential applications of BCP thin films to different nanotechnologies have been developed, such as the BCP lithography,[5–8] nanoparticle template,[9–12] nanoarray,[13–17] and nano-

porous thin film.[18–21] One of the appealing applications to nanopatterning is to utilize the self-assembled BCP nanostructure in the thin film as a mask to generate inorganic nanoarrays and nanoporous thin films.

Polymeric materials comprising inorganic components, such as polydimethylsiloxane (PDMS) which can readily form silicon oxide under an oxygen plasma environment or under ultraviolet (UV) exposure with ozone treatment, have been extensively studied because of their potential applications.[22,23] The silicon-containing materials can form a thin silicon oxide layer which can resist further etching by oxygen plasma. This silicon oxide layer is responsible for the low etching rate of the silicon-containing material as compared to that of the polymers which only contain C, H, N, and O atoms. Combining an easily etchable block with a silicon-containing block can provide good etching selectivity. This etching selectivity provides the basis for most of the multilayer resist schemes involving pattern transfer. Since BCPs can self-assemble into a variety of nanostructures by varying the molecular weight and composition of the individual blocks, the self-assembly of silicon-containing BCPs can be employed for nanopatterning. A number of studies with respect to silicon-containing BCPs for various applications have been reported.[8,24–32] For example, Thomas and co-workers demonstrated that PS-PDMS BCPs can be used as templates for the formation of silicon oxide nanoobjects in bulk with the use of oxygen plasma or exposure to UV light with ozone treatment.[22] Ross and co-workers demonstrated the feasibility of nanolithographic applications by using PS-PDMS BCPs.[26,27] With the combi-

nation of different technologies including graphoepitaxy, solvent annealing, metal sputtering, and dry etching, the fabrication of various nanoporous metallic thin films using a mask from PS-PDMS BCP thin film could be achieved.[27]

In contrast to the fabrication of inorganic nanoporous thin films, we aim to fabricate nanoporous polymeric thin films. Here, we use a one-step oxidation process in PS-PDMS BCP thin films to simultaneously etch the minor PS component into thru-pore nanochannels and to convert the PDMS matrix into a robust inorganic film. Well-defined ultrathin freestanding nanoporous films with hexagonally packed nanochannels can be obtained through the BCP self-assembly using a PS-PDMS BCP with 33 vol % PS by content and 34.7 kg/mol total molecular weight. The dimension of the nanochannels is approximately 16 nm, well below the feature size from the typical regular top-down method. Subsequently, these films can be used as contact masks for pattern transfer into various underlying substrates by suitable etching to generate various nanoporous polymeric materials. Moreover, our porous mask films are freestanding for pattern transfer so that they are reusable, providing an easy and highly selective-etching process to produce topographic polymeric patterns.

RESULTS AND DISCUSSION

PS-PDMS BCPs were synthesized through sequential anionic polymerization to form cylindrical PS domains in a PDMS matrix. As illustrated in Figure 1a, a thin-film sample is prepared by spin coating from dodecane solution (1 wt % of PS-PDMS) onto a carbon-coated glass slide. Subsequently, the PS-PDMS thin film is removed from the glass substrate using 1% HF solution and then floated onto water (Figure 1b). A copper TEM grid is used to pick up the PS-PDMS thin-film which is then dried in a vacuum oven for 12 h (Figure 1c). Finally, a freestanding silicon oxy carbide thin film with cylinder-forming nanochannels is obtained by treating the BCP film with oxygen plasma (Figure 1d) whereby the PS cylinders are removed and the thin carbon substrate is also removed.

Figure 2a shows the scanning probe microscopy (SPM) height image of the spin-coated PS-PDMS thin film in which vertically oriented cylindrical PS domains can be obtained. As determined by SPM, the pristine BCP thin film possesses hexagonally packed PS cylinders having a diameter of approximately 18 nm and center-to-center distance of approximately 31 nm. To analyze the film surface composition of the PS-PDMS BCP, X-ray photoelectron spectroscopy (XPS) was carried out, similar to the approach reported by Nealey and co-workers.[33] The XPS shows the atomic composition of the film surface as well as the estimated volume ratio of constituent block exposed to the film surface (see Figure S1 of the Supporting Information (SI)). The surface composition of the silicon area in the pristine BCP
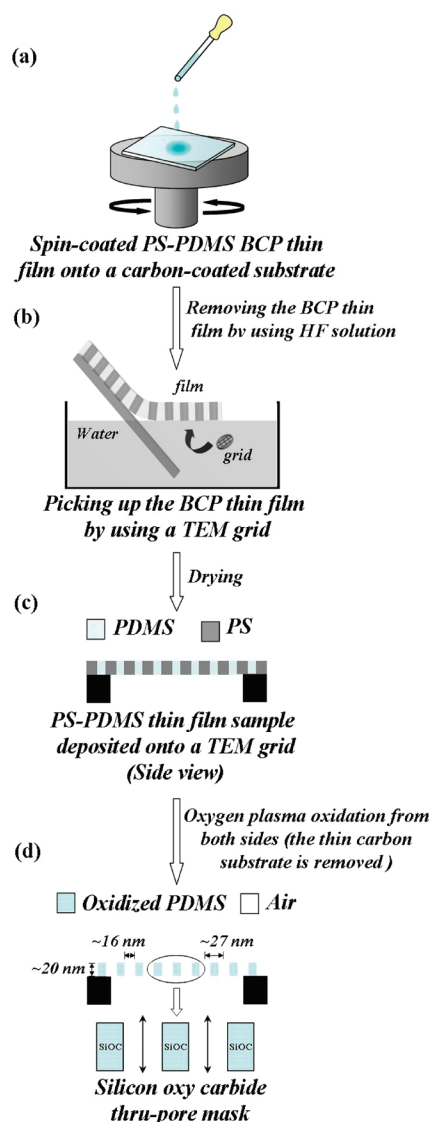

Figure 1. Schematic illustration of the preparation of silicon oxy carbide thru-pore mask.

thin film was approximately 0.7 in weight by using the silicon area of PDMS homopolymer as standard (see Table S1 of SI). Consistently, it is very close to the constituted fraction of PDMS in the PS-PDMS BCP synthesized. Figure 2b shows a top-view field-emission scanning electron microscopy (FESEM) image of the nanoporous thin film deposited onto a copper grid after the oxygen plasma treatment. The copper grid with a $40 \times 40 \ \mu m^2$ area is completely covered by the nanoporous thin film (see Figure S2 of SI). In addition to the top-view image, the bottom-view image also shows a similar nanoporous texture, implying that the cylindrical nanochannels run through the entire thickness of the thin film (see Figure S3 of SI). Furthermore, the thin-film sample is observed by TEM (Figure 2c); the TEM micrograph having bright pore regions in contrast to the dark matrix further confirms the formation of the nanopore texture at which the PS domain is removed by
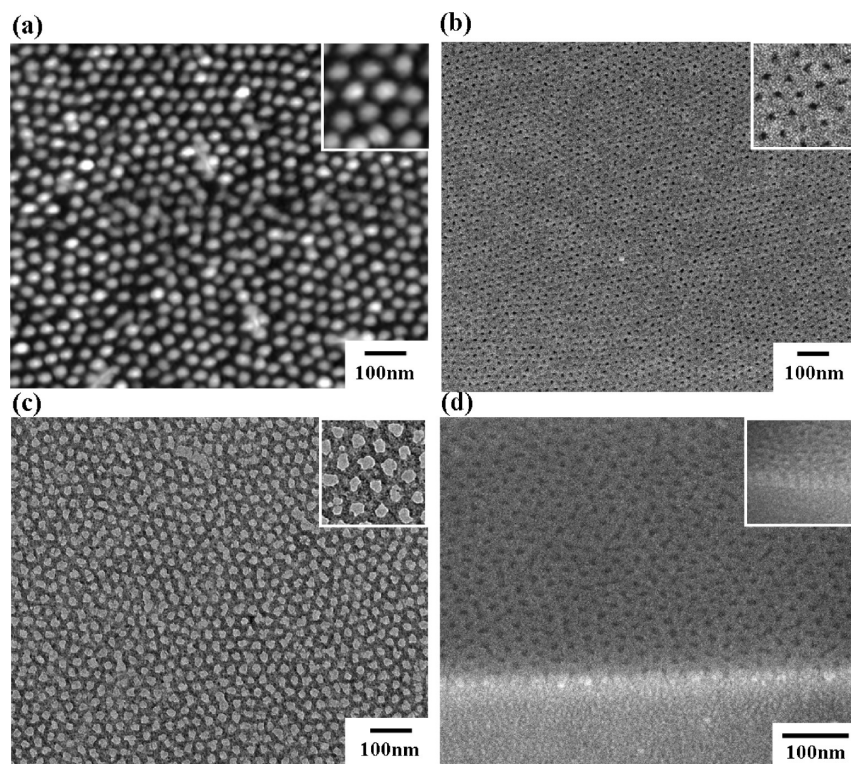
Figure 2. (a) Tapping-mode AFM height image of spin-coated PS-PDMS thin film and the inset shows the enlarged area, **(b)** top-view FESEM image of nanoporous thin film and the inset shows the enlarged area, **(c)** TEM image of nanoporous thin film and the inset shows the enlarged area, **(d)** cross-section-view FESEM image of nanoporous thin film on wafer for the 45° tilt angle and the inset shows the enlarged area at higher tilt angle.

the oxygen plasma treatment. Also, the pore diameter of the oxidized PS-PDMS thin film was determined as 16 nm in average, as determined by TEM observation. The pore diameter on the surface of the oxidized film is measured as being approximately equal to that of the pristine PS domain. Most importantly, the cross-section-view FESEM image of the film (Figure 2d) clearly demonstrates that the perpendicular cylindrical nanochannels truly span the thickness of the 20 nm thin film.

To investigate the chemical nature of the oxidized PS-PDMS thin-film sample, XPS was used to investigate the conversion of the PDMS block and the removal of the PS block.[34,35] For comparison, a PDMS homopolymer thin-film sample was also prepared for XPS examination. As shown in Figure 3a, the characteristic Si 2p peak of silicon in the PS-PDMS BCPs and PDMS homopolymer can be identified at 102 eV. After the oxygen plasma treatment, the XPS study showed a shift to a higher binding energy of the Si 2p peak. Moreover, the intensity of O 1s peak for the PS-PDMS BCPs at 532 eV increases (Figure 3b). The oxygen-plasma-treated PDMS homopolymer exhibits similar behavior to the PS-PDMS BCPs (results not shown). Those results clearly indicate the occurrence of PDMS oxidation. Also, the C 1s peak at 285 eV broadens, and its intensity decreases, but not annihilation after the oxygen plasma treatment (Figure 3c). As a result, we suggest that the PS-
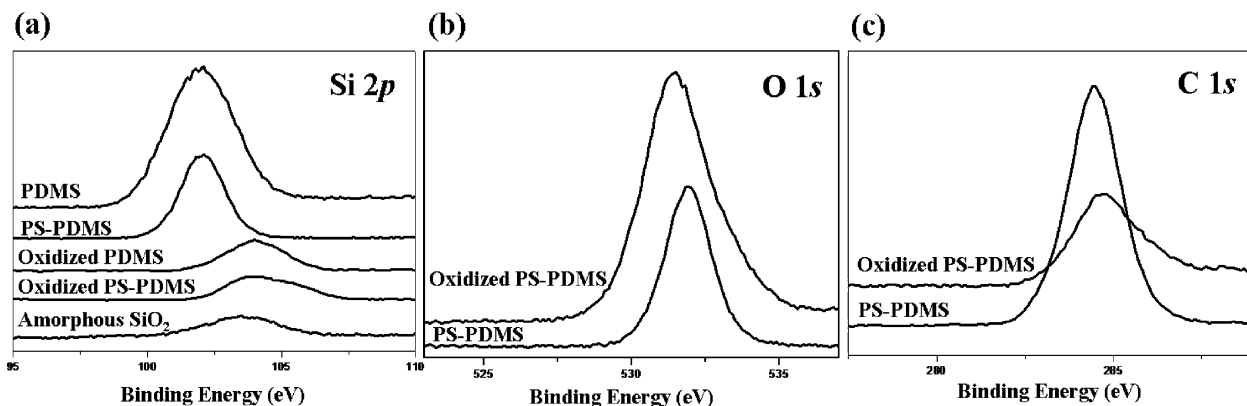

Figure 3. XPS spectra of **(a)** Si 2p of PDMS homopolymer, PS-PDMS, oxidized PDMS homopolymer, oxidized PS-PDMS thin films, and amorphous SiO_2; **(b)** O 1s and **(c)** C 1s of PS-PDMS and oxidized PS-PDMS thin films.
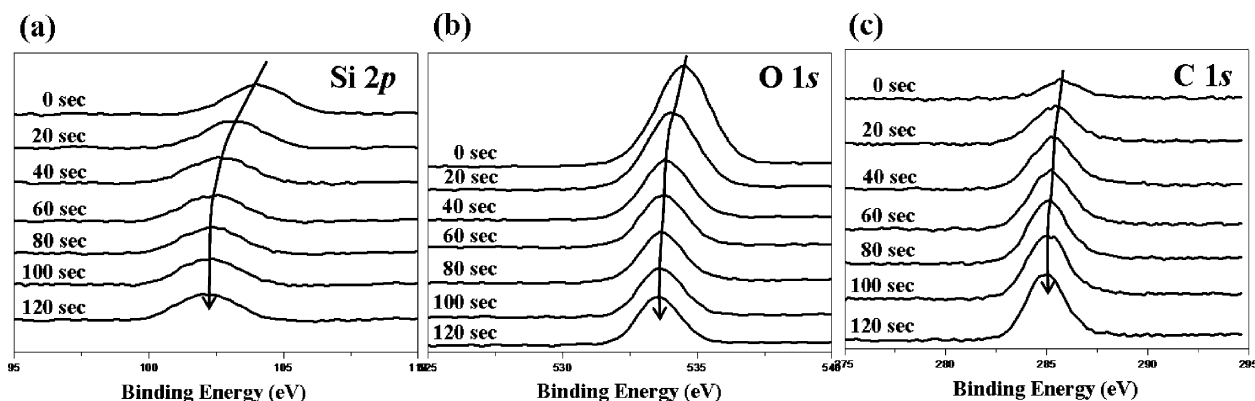
Figure 4. XPS spectra of the oxidized PDMS homopolymer thin film: (a) Si 2p; (b) O 1s; (c) C 1s. The time in the figure indicates the duration of the argon ion sputtering, and the etching rate is roughly estimated to be 0.1 nm sec^{-1}.

PDMS thin film is oxidized to form silicon oxy carbide after the oxygen plasma treatment.

The thickness of oxidized layer in the self-assembled BCPs is critical for applications. To resolve the oxidized depth of the PDMS domains by the oxygen plasma treatment, argon ion sputtering experiments were carried out to examine the thickness of oxidized PDMS in a homopolymer thin film. By taking advantage of surface etching through the argon ion sputtering in the normal direction of the film, a depth profile with respect to the binding energy analysis can be achieved with excellent depth resolution. After the sequential argon ion sputtering, the oxidized PDMS thin-film sample was examined by XPS to trace the change of the binding energy at different depths of the thin film. Figure 4 shows the XPS spectra of Si 2p, O 1s, and C 1s in the oxidized films at different times of argon ion sputtering. Before the argon ion sputtering (*i.e.*, the examination of uppermost oxidized surface), the Si 2p has a peak at 104 eV (Figure 4a) and the O 1s and C 1s (Figure 4b,c) signals appear at 534 and 285 eV, respectively. When the argon ion sputtering occurs, the Si 2p peak gradually shifts to low binding energy. Simultaneously, the intensity of the C 1s peak increases as the etching time increases, whereas the intensity of the O 1s peak decreases. After 100 s of argon ion sputtering, the Si 2p peak shifts to 102 eV (the binding energy of the silicon atoms in pristine PDMS), whereas the O 1s and C 1s peaks essentially remain. These results indicate that the oxidation of the PDMS homopolymer under the oxygen plasma treatment experiences a depth limitation. On the basis of a sputtering rate of 0.1 nm sec^{-1}, the PDMS homopolymer is estimated to possess approximately a 10 nm thickness of the oxidized PDMS thin film according to the occurrence of the shifting of Si 2p peak maxima.[36] For the PS-PDMS thin-film samples prepared in this study, the original film thickness was estimated at approximately 20 nm. Therefore, since oxidation occurs from both sides of the film, it is reasonable to assume that the PDMS oxidation is extensively completed.

Owing to the selective degradability of one component of BCPs under certain reactive conditions, such as

polystyrene-*b*-polyisoprene (PS-PI),[5,37] polystyrene-*b*-poly(methylmethacrylate) (PS-PMMA),[38,39] and polystyrene-*b*-poly(lactide) (PS-PLA),[24,40] *etc.*, BCPs can be used to prepare nanoporous thin-film templates. However, in contrast to the selectively degradable BCPs used for one-time topographic nanopatterning, the PS-PDMS BCPs can have multiple-use advantages since the inorganic nanoporous matrix from the oxidation of the PDMS is etch-resistant silicon oxy carbide. By taking advantage of the robust nanoporous silicon oxy carbide film, the film can be used as a mask for pattern transfer by oxygen reactive ion etching (RIE). In contrast to the oxygen plasma treatment, the oxygen RIE can provide an anisotropic etching direction to excellently transfer the feature of the mask into underlying substrates. We applied RIE at a RF-power of 75 W for 10 s in order to transfer the hexagonally packed cylinder-forming nanochannels into PS, PMMA, and PC (polycarbonate) substrates. As shown in Figure 5a−c, patterns can be successfully transferred to PS, PMMA, and PC with the features corresponding to the nanostructure of the nanoporous thin film. To examine the etching thicknesses of PS, PMMA, and PC thin films under the RIE treatment, the change of film thickness was measured after the same etching conditions for pattern transfer. The etching thicknesses of the PS, PMMA, and PC are 14.6, 22.3, and 12.6 nm, respectively, as determined by profilometer. Importantly, because of the robust nanoporous silicon oxy carbide mask with the high etching selectivity between the mask and polymeric materials under the oxygen RIE, this thin-film mask can be repeatedly used for pattern transfer. Figure 5d shows the freestanding mask after more than 30 pattern transfer processes; no significant change with respect to the texture and size can be recognized. This approach thus suggests an easy method to provide simple, convenient, reusable, and cost-effective ways to create nanoporous polymeric materials. Moreover, the nanoporous thin films could be very useful in many application fields such as separation membranes and catalyst support. Also, these nanoporous thin films exhibit significant potential in high heat transfer efficiency
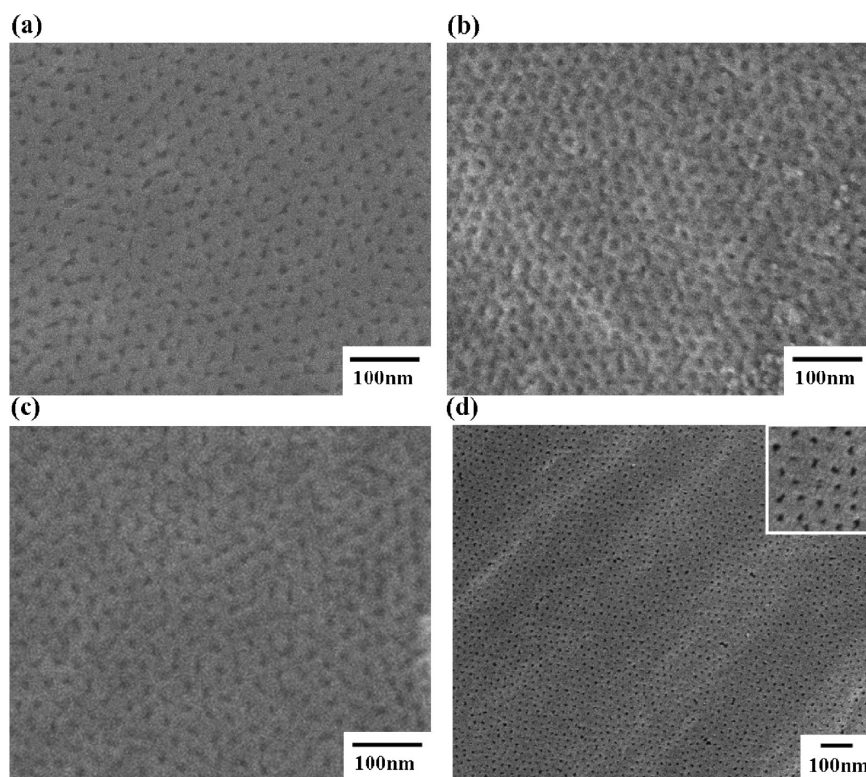
Figure 5. Top-view FESEM images of (a) PS, (b) PMMA, and (c) PC topographic nanopatterns created by using the silicon oxy carbide nanoporous mask for pattern transfer. (d) Top-view FESEM image of the mask after using the mask for more than 30 pattern transfers; the inset shows the enlarged area.

and evaporation because of the porosity and specific surface area from the nanoscale porous texture.[41,42]

CONCLUSIONS

Well-ordered cylinders with perpendicular orientation from the PS-PDMS thin films can be obtained directly by spin coating, and then transferred onto grids. A freestanding nanoporous thin film (namely, the silicon oxy carbide thin film with cylinder-forming nanochannels) can be directly fabricated *via* the oxygen plasma treatment, and closely placed onto various polymeric substrates. This nanoporous film could be used as an etch-resistant and reusable mask for pattern transfer into underlying polymeric substrates to directly generate nanoporous polymeric materials. Most importantly, this silicon oxy carbide mask can be repeatedly used because of its robust property and high etching selectivity under the oxygen RIE. Consequently, as demonstrated, topographic thin films of PS, PMMA, and PC can be obtained, providing an efficient way of nanofabrication to create topographic polymeric nanopatterns.

EXPERIMENTAL SECTION

A PS-PDMS BCP with PS cylinders in PDMS matrix was prepared through sequential anionic polymerization yielding $M_{n,PS}$ = 12.0 kg mol^{-1}, $M_{n,PDMS}$ = 22.7 kg mol^{-1}, and M_w/M_n = 1.04. Detailed synthetic routes for the preparation of PS-PDMS samples are described in the Supporting Information. Thin film samples were spin-coated onto a silicon wafer from 1 wt % dilute solution of PS-PDMS in dodecane at 2500 rpm and then observed by atomic force microscopy (AFM). A Seiko SPA-400 AFM with a SEIKO SPI-3800N probe station was employed at room temperature, and the tapping mode AFM images were obtained from thin-film samples. Field emission scanning electron microscopy was performed on a JEOL JSM-7401F using accelerating voltages of 3 keV. For the preparation of a shadow mask by using the PS-PDMS BCP thin film, the thin film was spin-coated on carbon-coated glass. Subsequently, the thin-film sample was removed from the glass substrate by using a HF solution and then floated onto a water surface. The PS-PDMS thin-film sample was picked up and deposited on a copper TEM grid where it dried in air overnight. Finally, the freestanding silicon oxy carbide thin film with cylinder-forming nanochannels can be obtained by the oxygen plasma treatment, where the carbon substrate is etched away. The oxygen plasma treatment for oxidation was carried out by a RF-power of 6.8 W at the pressure of 200 mtorr for 30 min. For pattern transfer experiments, both PS and PMMA thin films were spin-coated onto a silicon wafer from 1 wt % dilute solution in toluene at 1500 rpm. The PC samples were directly obtained from a commercial compact disk. Subsequently, the polymeric substrates were closely plastered with the freestanding mask. The RIE for pattern transfer was carried out by a RF-power of 75 W at the pressure of 75 mtorr for 10 s; the gas utilized in the etching process was oxygen produced by the flow rate of 1 sccm. XPS measurements were performed using a Thermo VG-Scientific Sigma Probe spectrometer equipped with a hemispherical electron analyzer. The operating conditions for XPS were as follows: Mg Kα anode, 15 kV, 7.2 mA; angle of collection, 45°; analysis diameter, 400 μm; sputter crater, 1 mm^2; Ar$^+$ ion beam energy, 3 keV, 1 μA; the sputtering rate was 0.1 nm sec^{-1}.

Supporting Information Available: Text giving detailed synthetic route of the PS-PDMS block copolymer. This material is available free of charge *via* the Internet at http://pubs.acs.org.

REFERENCES AND NOTES

1. Segalman, R. A. Patterning with block copolymer thin films. *Mater. Sci. Eng., R* **2005**, *48*, 191–226.
2. Darling, S. B. Directing the self-assembly of block copolymers. *Prog. Polym. Sci.* **2007**, *32*, 1152–1204.
3. Park, C.; Yoon, J.; Thomas, E. L. Enabling nanotechnology with self assembled block copolymer patterns. *Polymer* **2003**, *44*, 6725–6760.
4. Cheng, J. Y.; Ross, C. A.; Smith, H. I.; Thomas, E. L. Templated self-assembly of block copolymers: Top-down helps bottom-up. *Adv. Mater.* **2006**, *18*, 2505–2521.
5. Park, M.; Harrison, C.; Chaikin, P. M.; Register, R. A.; Adamson, D. H. Block copolymer lithography: Periodic arrays of ~1011 holes in 1 square centimeter. *Science* **1997**, *276*, 1401–1404.
6. Spatz, J. P.; Herzog, T.; Mobmer, S.; Ziemann, P.; Moller, M. Micellar inorganic−polymer hybrid systems—A tool for nanolithography. *Adv. Mater.* **1999**, *11*, 149–153.
7. Li, R. R.; Dapkus, P. D.; Thompson, M. E.; Jeong, W. G.; Harrison, C.; Chaikin, P. M.; Register, R. A.; Adamson, D. H. Dense arrays of ordered GaAs nanostructures by selective area growth on substrates patterned by block copolymer lithography. *Appl. Phys. Lett.* **2000**, *76*, 1689–1691.
8. Cheng, J. Y.; Ross, C. A.; Chan, V. Z. H.; Thomas, E. L.; Lammertink, R. G. H.; Vancso, G. J. Formation of a cobalt magnetic dot array *via* block copolymer lithography. *Adv. Mater.* **2001**, *13*, 1174–1178.
9. Lopes, W. A.; Jaeger, H. M. Hierarchical self-assembly of metal nanostructures on diblock copolymer scaffolds. *Nature* **2001**, *414*, 735–738.
10. Bockstaller, M. R.; Lapetnikov, Y.; Margel, S.; Thomas, E. L. Size-selective organization of enthalpic compatibilized nanocrystals in ternary block copolymer/particle mixtures. *J. Am. Chem. Soc.* **2003**, *125*, 5276–5277.
11. Darling, S. B.; Yufa, N. A.; Cisse, A. L.; Bader, S. D.; Sibener, S. J. Self-organization of FePt nanoparticles on photochemically modified diblock copolymer templates. *Adv. Mater.* **2005**, *17*, 2446–2450.
12. Lin, Y.; Boker, A.; He, J.; Sill, K.; Xiang, H.; Abetz, C.; Li, X.; Wang, J.; Emrick, T.; Long, S.; Wang, Q.; Balazs, A.; Russell, T. P. Self-directed self-assembly of nanoparticle/copolymer mixtures. *Nature* **2005**, *434*, 55–59.
13. Morkved, T. L.; Lu, M.; Urbas, A. M.; Ehrichs, E. E.; Jaeger, H. M.; Mansky, P.; Russell, T. P. Local control of microdomain orientation in diblock copolymer thin films with electric fields. *Science* **1996**, *273*, 931–933.
14. Kim, S. O.; Solak, H. H.; Stoykovich, M. P.; Ferrier, N. J.; de Pablo, J. J.; Nealey, P. F. Epitaxial self-assembly of block copolymers on lithographically defined nanopatterned substrates. *Nature* **2003**, *424*, 411–414.
15. Morikawa, Y.; Nagano, S.; Watanabe, K.; Kamata, K.; Iyoda, T.; Seki, T. Optical alignment and patterning of nanoscale microdomains in a block copolymer thin film. *Adv. Mater.* **2006**, *18*, 883–886.
16. Tseng, Y. -T.; Tseng, W. -H.; Lin, C. -H.; Ho, R. -M. Fabrication of double-length-scale patterns *via* lithography, block copolymer templating, and electrodeposition. *Adv. Mater.* **2007**, *19*, 3584–3588.
17. Park, S.; Kim, B.; Wang, J. -Y; Russell, T. P. Fabrication of highly ordered silicon oxide dots and stripes from block copolymer thin films. *Adv. Mater.* **2008**, *20*, 681–685.
18. Chan, V. Z. H.; Hoffman, J.; Lee, V. Y.; Iatrou, H.; Avgeropoulos, A.; Hadjichristidis, N.; Miller, R. D.; Thomas, E. L. Ordered bicontinous nanoporous and nanorelief ceramic films from self assembling polymer precursors. *Science* **1999**, *286*, 1716–1719.
19. Zalusky, A. S.; Olayo-Valles, R.; Taylor, C. J.; Hillmyer, M. A. Mesoporous polystyrene monoliths. *J. Am. Chem. Soc.* **2001**, *123*, 1519–1520.
20. Yang, S. Y.; Ryu, I.; Kim, H. Y.; Kim, J. K.; Jang, S. K.; Russell, T. P. Nanoporous membranes with ultrahigh selectivity and flux for the filtration of viruses. *Adv. Mater.* **2006**, *18*, 709–712.
21. Olson, D. A.; Chen, L.; Hillmyer, M. A. Templating nanoporous polymers with ordered block copolymers. *Chem. Mater.* **2008**, *20*, 869–890.
22. Chan, V. Z. H.; Thomas, E. L.; Lee, V. L.; Miller, R. D.; Avgeropoulos, A.; Hadjichristidis, N. Periodic porous and relief nanostructure articles. U.S. Patent Publication No: WO/00/02090.
23. Brinkmann, M.; Chan, V. Z. H.; Thomas, E. L.; Lee, V. L.; Miller, R. D.; Hadjichristidis, N.; Avgeropoulos, A. Room-temperatures synthesis of α-SiO_2 thin films by UV-assisted ozonolysis of a polymer precursor. *Chem. Mater.* **2001**, *13*, 967–972.
24. Ndoni, S.; Vigild, M. E.; Berg, R. H. Nanoporous materials with spherical and gyroid cavities created by quantitative etching of polydimethylsiloxane in polystyrene−polydimethylsiloxane block copolymers. *J. Am. Chem. Soc.* **2003**, *125*, 13366–13367.
25. Li, L.; Yokoyama, H. Nanoscale silica capsules ordered on a substrate: Oxidation of nanocellular thin films of poly(styrene-*b*-dimethylsiloxane). *Angew. Chem., Int. Ed.* **2006**, *45*, 6338–6341.
26. Jung, Y. S.; Ross, C. A. Orientation-controlled self-assembled nanolithography using a polystyrene−polydimethylsiloxane block copolymer. *Nano Lett.* **2007**, *7*, 2046–2050.
27. Jung, Y. S.; Ross, C. A. Well-ordered thin-film nanopore arrays formed using a block-copolymer template. *Small* **2009**, *5*, 1654–1659.
28. Rider, D. A.; Cavicchi, K. A.; Vanderark, L.; Russell, T. P.; Manners, I. Orientationally controlled nanoporous cylindrical domains in polystyrene-*b*-poly(ferrocenylethylmethylsilane) block copolymer films. *Macromolecules* **2007**, *40*, 3790–3796.
29. Rider, D. A.; Liu, K.; Eloi, J. -C.; Vanderark, L.; Yang, L.; Wang, J. -Y.; Grozea, D.; Lu, Z. -H.; Russell, T. P.; Manners, I. Nanostructured magnetic thin films from organometallic block copolymers: Pyrolysis of self-assembled polystyrene-*block*-poly(ferrocenylethylmethylsilane). *ACS Nano* **2008**, *2*, 263–270.
30. Bita, I.; Yang, J. K. W.; Jung, Y. S.; Ross, C. A.; Thomas, E. L.; Berggren, K. K. Graphoepitaxy of self-assembled block copolymers on two-dimensional periodic patterned templates. *Science* **2008**, *321*, 939–943.
31. Jung, Y. S.; Jung, W.; Ross, C. A. Nanofabricated concentric ring structures by templated self-assembly of a diblock copolymer. *Nano Lett.* **2008**, *8*, 2975–2981.
32. Jung, Y. S.; Jung, W.; Tuller, H. L.; Ross, C. A. Nanowire conductive polymer gas sensor patterned using self-assembled block copolymer lithography. *Nano Lett.* **2008**, *8*, 3776–3780.
33. Son, J. G.; Bae, W. K.; Kang, H.; Nealey, P. F.; Char, K. Placement control of nanomaterial arrays on the surface-reconstructed block copolymer thin films. *ACS Nano* **2009**, *3*, 3927–3934.
34. Chou, N. J.; Tang, C. H.; Paraszczak, J.; Babich, E. Mechanism of oxygen plasma of polydimethyl siloxane films. *Appl. Phys. Lett.* **1985**, *46*, 31–33.
35. Hartney, M. A.; Chiang, J. N.; Hess, D. W.; Soane, D. S. Oxide formation during plasma etching of silicon-containing resists. *Appl. Phys. Lett.* **1989**, *54*, 1510–1512.
36. The Ar sputtering rate was in accordance with the measurement manual of Thermo VG-Scientific Sigma Probe spectrometer.

37. Park, M.; Chaikin, P. M.; Register, R. A.; Adamson, D. H. Large area dense nanoscale patterning of arbitrary surfaces. *Appl. Phys. Lett.* **2001**, *79*, 257–259.

38. Thurn-Albrecht, T.; Steiner, R.; DeRouchey, J.; Stafford, C. M.; Huang, E.; Bal, M.; Tuominen, M.; Hawker, C. J.; Russell, T. P. Nanoscopic templates from oriented block copolymer films. *Adv. Mater.* **2000**, *12*, 787–790.

39. Zschech, D.; Kim, D. H.; Milenin, A. P.; Scholz, R.; Hillebrand, R.; Hawker, C. J.; Russell, T. P.; Steinhart, M.; Gösele, U. Ordered arrays of ⟨100⟩-oriented silicon nanorods by CMOS-compatible block copolymer lithography. *Nano Lett.* **2007**, *7*, 1516–1520.

40. Olayo-Valles, R.; Guo, S.; Lund, M. S.; Leighton, L. C.; Hillmyer, M. A. Perpendicular domain orientation in thin films of polystyrene−polylactide diblock copolymers. *Macromolecules* **2005**, *38*, 10101–10108.

41. Johnson, D. W.; Yavuzturk, C.; Pruis, J. Analysis of heat and mass transfer phenomena in hollow fiber membranes used for evaporative cooling. *J. Membr. Sci.* **2003**, *227*, 159–171.

42. Traum, M. J.; Griffith, P.; Thomas, E. L.; Peters, W. A. Latent heat fluxes through soft materials with microtruss architectures. *J. Heat Transfer* **2008**, *130*, 042403.